



Full length article

Improving WRF-Chem PM_{2.5} predictions by combining data assimilation and deep-learning-based bias correction

Xingxing Ma, Hongnian Liu*, Zhen Peng

School of Atmospheric Sciences, Nanjing University, Nanjing 210023, China

ARTICLE INFO

Keywords:
 WRF-Chem
 Bias correction
 Data assimilation
 PM_{2.5} concentrations
 Optimization

ABSTRACT

In numerical model simulations, data assimilation (DA) on the initial conditions and bias correction (BC) of model outputs have been proven to be promising approaches to improving PM_{2.5} (particulate matter with an aerodynamic equivalent diameter of $\leq 2.5 \mu\text{m}$) predictions. This study compared the optimization effects of these two methods and developed a new scheme that combines DA and BC simultaneously. Four parallel experiments were conducted during winter 2019: a control experiment directly forecasted by WRF-Chem (experiment name: WRF-Chem); an experiment that assimilated *in situ* observations based on the GSI (Gridpoint Statistical Interpolation) system (WRF-Chem_DA); an experiment with deep-learning-based BC (WRF-Chem_BC); and an experiment considering the combination of DA on the initial conditions and BC (WRF-Chem_DA_BC). Statistically, the accuracy of PM_{2.5} predictions could be optimized by both DA and BC for the first 24-h period, and WRF-Chem_BC performed better than WRF-Chem_DA in the initial field, especially in the period of 10–24 h, while the best performance was achieved by combining BC and DA. Throughout the initial 24-h period, compared with the control experiment, the results of WRF-Chem_DA_BC (WRF-Chem_DA, WRF-Chem_BC) showed an improvement in terms of root-mean-square error, with reduction proportions varying from 38.90 % to 48.86 % (18.88 % to 32.44 %, 30.10 % to 46.08 %). Besides having the best optimization effect over the whole domain, the combined method also performed well in different regions: during the forecasting period of 0–24 h, the RMSEs decreased from 32 % to 62 %, 39 % to 57 %, 28 % to 40 %, and 30 % to 49 % in the Beijing–Tianjin–Hebei, Yangtze River Delta, Central China, and Sichuan Basin urban agglomerations, respectively.

1. Introduction

China's recent rapid socioeconomic development has brought with it some serious air pollution problems. Studies have shown that, among all atmospheric pollutants, PM_{2.5} (particulate matter with an aerodynamic equivalent diameter of $\leq 2.5 \mu\text{m}$) is of particular concern because of its effects on human health (Kampa and Castanas, 2008; Pope et al., 2011; Teng et al., 2023; Li et al., 2023). In addition, it also makes important contributions to hazy weather in autumn and winter, causing reduced visibility and inconvenience to transportation (Jiang et al., 2012; Ma et al., 2020). Therefore, the Chinese government has introduced a series of initiatives, such as the "Three-year Plan of Action for Winning the War to Protect Blue Skies", to combat pollution of PM_{2.5} and other pollutants in urban agglomerations (Guo et al., 2017; Wang et al., 2017; Teng et al., 2023).

In order to better manage and prevent air pollution processes, it is important to improve the prediction accuracy for pollutants such as

PM_{2.5}, based on numerical models (Chen et al., 2017; Ma et al., 2020). Numerical models mainly realize their forecasts by combining the consideration of pollutant emissions, meteorological conditions, and physicochemical reactions. With the continuous research and development of numerical models, many regional and global atmospheric chemistry models, such as the Weather Research and Forecasting model coupled with Chemistry (WRF-Chem; Grell et al., 2005), the Community Multiscale Air Quality model (CMAQ, <https://www.epa.gov/cmaq>), the Nested Air Quality Prediction Modeling System (NAQPMS; Wang et al., 2001), and the Global Modeling and Assimilation Office (GEOS-Chem, <https://www.geos-chem.org>), have been developed in recent years. However, due to the considerable uncertainties and model assumptions related to pollutant emissions, meteorological conditions, and chemical reaction mechanisms, the frameworks and parameterization schemes of these models are still imperfect, which may bring errors in their forecasts (Van Loon et al., 2007; Zhu et al., 2018; Lv et al., 2018).

In the fall and winter, when heavy pollution events are at their most

* Corresponding author.

E-mail address: liuhn@nju.edu.cn (H. Liu).

frequent, the model forecast bias of PM_{2.5} is relatively higher, and can even exceed 30 % (Gao et al., 2016; Lu et al., 2020). In order to reduce model prediction errors and improve the forecast accuracy, certain methods have been proposed such as data assimilation (DA), model parameter optimization, bias correction (BC), and emission optimization with DA. DA can reduce the uncertainty of the chemical initial field and source emission to improve the prediction accuracy; BC can be used to construct a relationship between historical observations and the corresponding model forecasts to realize correction of model predictions and thus reduce prediction errors.

The inverse optimization method such as the ensemble Kalman filter (EnKF) for emission sources was proposed to calibrate the emission inventories, reducing the uncertainty of emission sources and improving the prediction accuracy (Fu et al., 2022; Zeng and Wu, 2022). Using the EnKF approach to assimilate ground-based PM_{2.5} observations, Peng et al. (2017) demonstrated the advantages of joint adjustment of the emission source and the initial field in improving the accuracy of PM_{2.5} forecasts. In their subsequent study, Peng et al. (2018a), Peng et al. (2018b) simultaneously performed joint assimilation optimization of emission sources with multiple elements to improve the forecasting of specific pollutant species. Ma et al. (2020) used the optimized EnKF system to assimilate ground-based observation elements and satellite-derived aerosol optical depth data to achieve enhancement of PM_{2.5} forecasts.

DA on the initial conditions is an important technique to obtain an optimal analysis field to correct model uncertainties by combining the observation field with the model background field (Evensen, 2009; Chen et al., 2023; Shen et al., 2018). The analysis field shows advantages due to the fusion of both observation and background information, which can maintain the level of consistency with actual atmospheric observations (Ma et al., 2020). The analysis field can be used as the chemical initial field to improve the initial conditions and thus optimize the model predictions (Shen and Min, 2015; Shen et al., 2020; Wei et al., 2022; Jiang et al., 2013; Ma et al., 2018; Schwartz et al., 2012). The development of a global environmental monitoring network has provided the data foundation for DA, and *in situ* aerosol observations have been widely used in atmospheric chemistry DA due to their accessibility (Bocquenet et al., 2015; Ma et al., 2020).

Schwartz et al. (2012) used three different assimilation methods with MODIS (Moderate Resolution Imaging Spectroradiometer) AOD (aerosol optical depth) products and *in situ* PM_{2.5} observations, and the results showed that all three methods improved the forecasting of aerosols. Song et al. (2021) used the 3DVAR (three-dimensional variational) approach to jointly assimilate meteorological data and *in situ* observations to improve the prediction of PM_{2.5}. Hong et al. (2022) assimilated *in situ* observations and satellite data simultaneously to further improve PM_{2.5} predictions. And in another study, different kinds of data were used in the assimilation of the initial field to analyze the enhancement of PM_{2.5} forecasts by different assimilation sources (Ma et al., 2024). These previous studies have shown that DA can improve PM_{2.5} predictions by adjusting the initial state of the atmospheric chemistry, but the improvement of the prediction is limited, and the effect of assimilation gradually disappears with long-term integration of the simulation (Ma et al., 2024; Ma et al., 2020; Hong et al., 2022). In addition, the model prediction errors are not only affected by the uncertainty of the initial field, but also various other uncertainties such as those of the meteorological field and the physicochemical reactions (Zhu et al., 2018). Numerical model BC comprehensively considers the systematic errors of the model forecast to improve the forecast accuracy. Different from DA, which is the adjustment of the initial field from the model input perspective, BC is the post-processing of model outputs from the back end of the model, and can to a certain extent make up for the limitations of initial field DA.

BC is a statistical method that improves model predictions by establishing a relationship between historical observations and the corresponding model forecasts, from which the forecast bias can be

extracted and the systematic errors corrected. With the advancements made in this line of research, BC methods have been developed from the earlier complete forecast method (Klein et al., 1959) to the model output statistical method (Glahn and Lowry, 1972), and then gradually evolved into different BC schemes. Frequency matching, Bayesian averaging, least-squares regression, multiple linear regression, and other statistical methods have been used to establish BC models, which significantly reduce systematic errors by learning the empirical relationships between historical forecasts and observations to realize BC (Raftery et al., 2005; Zhu and Luo, 2015; Xie et al., 2012; Chen et al., 2012; You, 2014). Recently, artificial-intelligence machine-learning techniques have emerged. Subsequently, BC based on machine-learning methods has been shown to better express the auxiliary links between various facets of the atmosphere, including, for instance, the different elements involved in atmospheric chemistry and key basic meteorological variables such as temperature and winds (Marzban, 2003; Zhang et al., 2022). Machine-learning models have been used in the BC of model outputs to improve PM_{2.5} forecasts. For example, Ran et al. (2023) performed BC based on a multiple linear regression modeling approach to reduce the global PM_{2.5} prediction bias; and Liu and Xing (2022a), Liu and Xing (2022b) designed a fully connected deep neural network to correct the PM_{2.5} concentration bias in the outputs of chemical models, achieving better results than without the correction method applied. Ma et al. (2020) applied a time series model to correct PM_{2.5} forecasts, which achieved good results. Different machine-learning methods were utilized by Li et al. (2021) as bias adjustment for postprocessing forecasts of PM_{2.5} and O₃, showing the optimal approach to be the Random Forest model. Lu et al. (2020) utilized machine-learning methods to improve the accuracy of PM_{2.5} forecasts through WRF-Chem in the Chengdu–Chongqing region. Overall, machine-learning methods have shown strong advantages in mining nonlinear relationships, enabling them to perform well in the BC of numerical predictions. However, they usually require massive, multi-source data inputs, which can limit their applicability in specific scenarios.

It can be seen that DA on the initial conditions can optimize the forecast accuracy from the model input perspective through reducing the uncertainty of the initial field, while BC can make improvements to predictions by correcting and reducing the forecast errors from the post-processing point of view. Both methods can improve the accuracy level of pollutant forecasting to a certain extent. Although both methods can improve the forecast accuracy of the model from the perspective of data statistics, previous studies have tended to analyze the enhancement of model forecasts by the two methods independently, with few studies having compared the enhancement effects of these two methods together. In addition, the effect of combining DA on the initial conditions and BC on the optimization of the model forecast has not been studied.

The application of DA to adjust the initial field can improve the accuracy of forecasts from the input perspective of the model by reducing the uncertainty of the initial conditions, and then applying BC to the assimilated forecast results can further optimize the model forecast from the output perspective, which when combined simultaneously could be of great significance for prediction improvement. Therefore, in this study, we considered the two different techniques of DA on the initial conditions and BC separately, and compared their abilities to optimize and enhance the forecasting of PM_{2.5} concentrations. Besides, a new scheme that combines DA on the initial conditions and BC simultaneously was developed to further improve PM_{2.5} predictions. The winter of 2019 was selected as the study period, and different comparative experiments were designed to evaluate and analyze the effects on optimizing the PM_{2.5} concentration forecasts.

2. Data and methodology

2.1. Data

In this study, measurements of PM_{2.5} concentrations recorded from 1 January 2017 to 28 February 2019, at approximately 1691 stations in China, were collected from the website of the China National Environmental Monitoring Center. The hourly averages of PM_{2.5} concentrations during this study period were used as the real values for correction and evaluation of bias, and the missing data values and those values higher than 1000 µg/m³ were removed.

The meteorological boundary conditions and initial field were provided by the National Centers for Environmental Prediction Final operational global analysis data, with a spatial resolution of 0.25° × 0.25° and temporal resolution of 6 h. For the model matching, the Multiresolution Emission Inventory of China in 2016 (<https://meicmod.el.org.cn>), with grid spacing of 0.25° and temporal resolution of 1 month, was processed into gridded data to match the grid spacing of the model. The emission source contained nine major pollutants, including SO₂, NOx, CO, NMVOC, NH₃, PM₁₀, PM_{2.5}, BC, OC, and CO₂ (Li et al., 2017; Zheng et al., 2018). Besides, the biogenic emissions were also calculated, using the Model of Emissions of Gases and Aerosols from Nature inventory (Guenther et al., 2006). The boundary conditions and initial fields of the atmospheric chemistry were derived from a simulation with WACCM (Whole Atmosphere Community Climate Model; <https://www.acom.ucar.edu/waccm/download.shtml>).

2.2. WRF-Chem model configurations

The Weather Research and Forecasting (WRF) model coupled with chemistry, WRF-Chem v3.8, developed collaboratively by various atmospheric research institutes, was used in this study (Grell et al., 2005). WRF-Chem has been used in many previous studies for forecasting pollution, and proved to perform well in the simulation of PM_{2.5} (Hong et al., 2022; Jiang et al., 2013; Tie et al., 2009; Zhou et al., 2015).

The Rapid Radiative Transfer Model scheme (Mlawer et al., 1997) was used for longwave radiation, and the Dudhia scheme (Dudhia, 1989) for shortwave radiation. The pavement process scheme and boundary layer parameterization scheme were set as the Noah scheme (Chen and Dudhia, 2001) and Yonsei University scheme, respectively

(Hong et al., 2006). The Morrison 2-moment scheme was used for the microphysics parameterization (Morrison et al., 2009). In addition, we used the Regional Acid Deposition Mechanism for the chemical mechanisms, and Global Ozone Chemistry Aerosol Radiation and Transport was the aerosol scheme (Stockwell et al., 1990; Chin et al., 2002).

The model was set as a 27-km grid resolution with 232 × 182 horizontal grid spacing and 35 vertical levels. The simulation domain in China is shown in Fig. 1, with the center of the model at (32°N, 110°E), including four typical urban agglomerations: Beijing–Tianjin–Hebei (BTH), Central China (CC), the Sichuan Basin (SCB), and Yangtze River Delta (YRD). These regions, chosen as they were in Chen et al. (2022), are of broad concern owing to their relatively more severe pollution related to their high levels of urbanization and dense populations.

2.3. GSI 3DVAR system

Grid Statistical Interpolation (GSI) is a data analysis system that integrates global and regional variational assimilation techniques developed by NCEP (National Centers for Environmental Prediction), and it has been used for DA in operational forecasting in recent decades (Chen et al., 2023; Feng, 2018). GSI 3DVAR is almost the same as traditional 3D variational methods, which are based on the idea of variational DA. However, it shows advantages in its ability to deal with observations that have complex nonlinear relationships with atmospheric state model variables, thus making it possible to assimilate observations with nonlinear relations to atmospheric state quantities. In order to improve aerosol predictions, an aerosol assimilation module was integrated systematically into the GSI 3DVAR system (Pagowski et al., 2014). In this paper, the DA of the initial field is based on the GSI system at 00:00 UTC each day. The GSI system is fitted to the observation and model background field by minimizing the objective function, and the analytical field is the optimal solution for the minimal value of the objective function in equation (1):

$$J(x) = \frac{1}{2}(x - x_b)^T B^{-1} (x - x_b) + \frac{1}{2}[H(x) - y]^T R1^{-1} [H(x) - y] \quad (1)$$

Here, B represents the background error covariance matrix and $R1$ is the observation error covariance matrix. They both represent the weight of the contributions to the analysis field. x and x_b represent the analysis field and background field, respectively, and y represents the

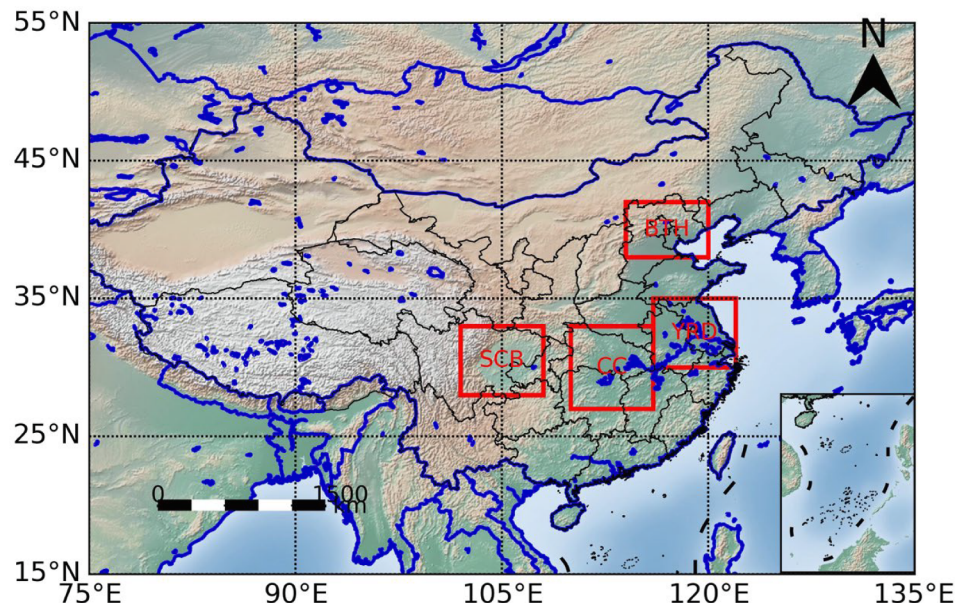


Fig. 1. The study area and its typical urban agglomerations. Abbreviations: SCB, Sichuan Basin; CC, Central China; YRD, Yangtze River Delta; BTH, Beijing–Tianjin–Hebei.

observations. H is the nonlinear observation operator that matches the model variables to the observations by interpolation. Similar to previous research, B is calculated with the NCEP NMC (National Meteorological Center) method (Rabier et al., 1998).

2.4. Deep-learning-based BC

By adding a multiscale convolution module and depth-separable module based on the classical UNet deep-learning segmentation network (Ronneberger et al., 2015), a new deep-learning method was constructed for BC of WRF-Chem predictions, named MDS-UNet (Ma et al., 2024). Actually, a multiscale convolution module was joined to connect and extract different scales of feature maps, and the depth-separable convolution can compress the feature mapping. MDS-UNet shows advantages in multiscale feature learning due to its multiscale convolution module, as compared with the traditional UNet. The single convolution kernel in the traditional model can only catch some of the features of the pollutants with a fixed scale. However, pollution characteristics vary on different spatial scales and multiscale convolution adopts a hierarchical structure with different spatial sizes of convolution kernels to extract the multiscale features by learning feature maps from the image. By merging feature maps of different scale, not only the pollutant concentration values, but also the spatial information on pollutant distributions, can then be obtained. The model has three advantages: acquisition of multiscale information, acquiring surrounding spatial information, and reducing information loss.

In BC model training, the loss function is important, which has been set here as in equation (2) to measure the disparity between the model output $\vec{y}_{b,m}$ and the real label $y_{b,m}$. Mean absolute error (MAE) and batch cross-entropy loss are commonly used in the model:

$$L_{HL} = L_{MAE} + \alpha L_{bcl} \quad (2)$$

where L_{MAE} is the MAE loss, L_{bcl} is the batch cross-entropy loss, and α is the loss allocation coefficient with a value of 0.001.

$$L_{bcl} = - \sum_{b=1}^B \sum_{m=1}^{Bn} p(y_{b,m}) \cdot \log \left(q(\vec{y}_{b,m}) \right) \quad (3)$$

$$L_{MAE} = \frac{\sum_{b=1}^B \sum_{m=1}^{Bn} \left| \vec{y}_{b,m} - y_{b,m} \right|}{Bn} \quad (4)$$

In equations (3) and (4), B is the batch size, Bn is the number of samples in the current batch, $p(y_{b,m})$ denotes the probability of the true

labeled value, $q(\vec{y}_{b,m})$ denotes the probability value of the model prediction, b represents the batch sample, and m represents the sample number in batch b .

2.5. Experimental design

The predictions during 0–24 h obtained directly from WRF-Chem and assimilated with the *in situ* observations of WRF-Chem + GSI were collected together with the observational data during January 2017 to November 2018 to form two separate training datasets. MDS-Unet was then used in the BC model construction for both the WRF-Chem and WRF-Chem + GSI predictions. The assimilation was conducted at 00:00 UTC and there was a 24-h simulation for each run. Four experiments, seen in Fig. 2, comprised (1) a control experiment directly using WRF-Chem (experiment name: WRF-Chem), (2) an experiment with assimilation of ground observations (WRF-Chem_DA), (3) an experiment with BC of WRF-Chem (WRF-Chem_BC), and (4) an experiment applying BC to a DA-applied model (WRF-Chem_DA_BC), in the study period of December 2018 to February 2019. To evaluate the effects of different methods on the performance of predictions, the root-mean-square error (RMSE), mean bias (MB), and correlation coefficient (R) were calculated as follows:

$$RMSE = \sqrt{\frac{1}{n} \sum_{i=1}^n (\vec{y}_i - y_i)^2} \quad (5)$$

$$MB = \frac{\sum_{i=1}^n |(\vec{y}_i - y_i)|}{n} \quad (6)$$

$$R = \frac{\sum_{i=1}^n (y_i - \bar{y})(\vec{y}_i - \bar{\vec{y}})}{\sqrt{\sum_{i=1}^n (y_i - \bar{y})^2 \sum_{i=1}^n (\vec{y}_i - \bar{\vec{y}})^2}} \quad (7)$$

MB and RMSE are metrics for assessing the errors between the predictions and observations, with a lower RMSE and MB indicating better model performance. In the equations, y_i is the observed value, \vec{y}_i is the predicted value, and n is the number of observations.

Pearson's R is used to reflect the agreement in variations between predictions and observations without considering the differences in magnitude. It ranges from -1 to 1, and a higher absolute value of R indicates a stronger linear relationship between observations and predictions. \bar{y} is the mean of the observed values, and $\bar{\vec{y}}$ is the mean of the predicted values.

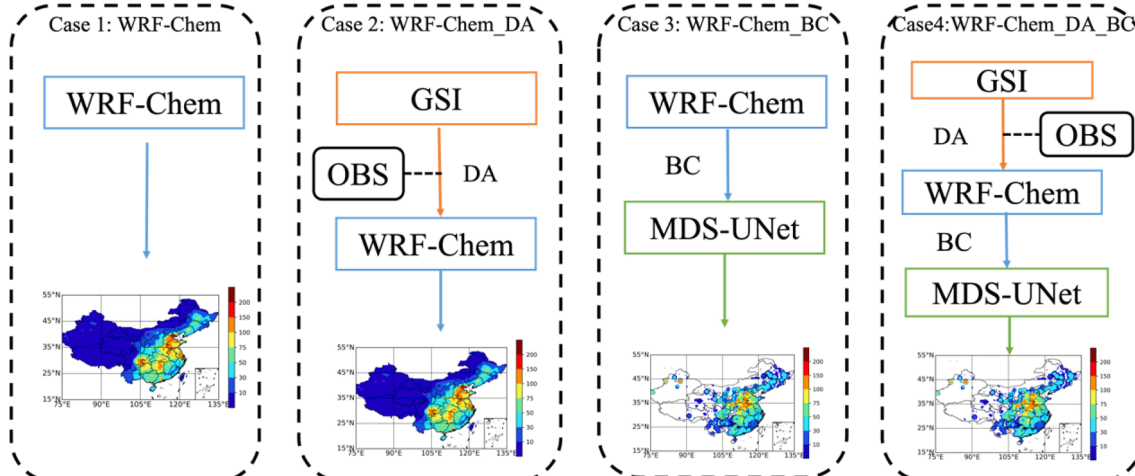


Fig. 2. Flow charts of the four different experiments. Case 1: WRF-Chem; Case 2: WRF-Chem_DA; Case 3: WRF-Chem_BC; Case 4: WRF-Chem_DA_BC.

$\text{PM}_{2.5}$ predictions with a dimension of 241 and 281 from WRF-Chem (WRF-Chem/GSI) during January 2017 to November 2018 were collected as the training dataset for experiment WRF-Chem_BC (WRF-Chem_DA_BC). The training dataset number was 13,982 with a temporal resolution of 1 h, and the testing dataset number was 1703 with the same temporal resolution. Besides, the observational dataset for the same period was interpolated using the “inverse distance weight” to form as the grid dataset. The numerical model output data was also interpolated to the equal latitude and longitude dataset to match with above obtained observation grid dataset.

3. Results and analysis

3.1. Comparison of forecast errors by different optimization methods

DA on the initial conditions improved the prediction accuracy by adjusting the initial field to optimize the model input, and BC made improvements by correcting the biases of the model output, which realized model optimization from different perspectives. The different improvements on the predictions achieved through DA and BC were evaluated with different error indicators. Fig. 3 shows the spatial performances of $\text{PM}_{2.5}$ prediction RMSEs averaged in winter produced by the different experiments. The prediction RMSEs in the control experiment were larger than those in the other three experiments, with high values mainly in BTH, YRD, CC, and some southwestern regions, and the RMSE even reached $100 \mu\text{g}/\text{m}^3$ in some northern areas. By comparing Fig. 3a, 3b and 3c, it can be seen that both DA and BC were able to reduce the $\text{PM}_{2.5}$ prediction RMSE, despite different performances over different regions. Compared with the control experiment, the prediction RMSE in WRF-Chem_DA was $20\text{--}40 \mu\text{g}/\text{m}^3$ lower over CC and YRD, while the DA improvements were small over BTH, where large RMSE values could still be seen. In contrast, the performances of BC were much better than those of DA, showing RMSE reductions over most areas in China, and the RMSE values were less than $80 \mu\text{g}/\text{m}^3$ in the WRF-Chem_BC experiment. Thus, by combining DA and BC, the best improvements were yielded, showing the largest reductions in prediction RMSE, with values less than $60 \mu\text{g}/\text{m}^3$, in the WRF-Chem_DA_BC

experiment (Fig. 3d). Overall, from the perspective of the RMSE distribution, WRF-Chem_DA_BC performed best in terms of the improvement of $\text{PM}_{2.5}$ predictions, followed by WRF-Chem_BC and then WRF-Chem_DA.

Fig. 4 presents the mean bias distributions of $\text{PM}_{2.5}$ predictions produced by the different experiments. As can be seen, WRF-Chem overestimated the $\text{PM}_{2.5}$ concentrations over some areas of SCB, CC, and YRD, with the prediction MB values reaching $60 \mu\text{g}/\text{m}^3$ in some areas. A reason for this might be that the emissions inventory overestimated the winter emissions in the above regions and the model simulation was relatively more uncertain due to the complex terrain (Wei et al., 2022). In contrast, the $\text{PM}_{2.5}$ concentrations were underestimated in BTH, with the prediction MB ranging from -60 to $-20 \mu\text{g}/\text{m}^3$. This performance whereby WRF-Chem always underestimates $\text{PM}_{2.5}$ concentrations over northern areas in China is a common problem, caused by not simulating secondary aerosols or the transformation mechanisms with their gaseous precursors (Ma, 2020; Wei et al., 2022; Qin et al., 2020; Wang et al., 2016). The prediction MB values were reduced by the DA and BC methods, but BC had better effects in terms of prediction improvement. Consistent with the results shown in Fig. 3, despite the adjustment to the original overestimation by DA in WRF-Chem_DA over some regions of SCB and CC, the prediction MB values could still reach $60 \mu\text{g}/\text{m}^3$ in some areas, thus demonstrating some advantages of DA, but with limitations. Compared with the direct predictions of WRF-Chem, the prediction MB values in the WRF-Chem_BC experiment were reduced over most areas due to BC effects. It is worth noting that the original overestimation changed to an underestimation in the WRF-Chem_BC experiment over some regions of YRD and the Shandong Peninsula, which indicated overcorrection by BC. For WRF-Chem_DA_BC, the prediction MB was the smallest among all the experiments, with values less than $20 \mu\text{g}/\text{m}^3$ over most areas. WRF-Chem_DA_BC showed a smaller prediction MB than WRF-Chem_BC, especially over the Shandong Peninsula and YRD regions.

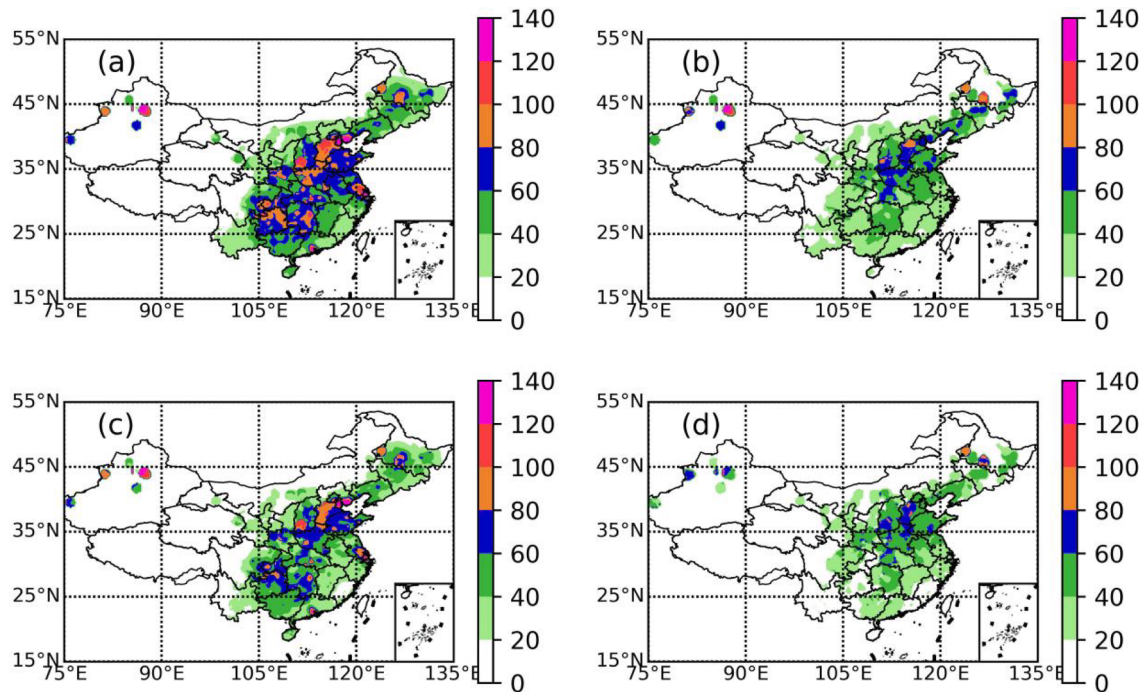


Fig. 3. Spatial distribution of the $\text{PM}_{2.5}$ prediction RMSE ($\mu\text{g}/\text{m}^3$) during winter produced by the four experiments: (a) WRF-Chem, (b) WRF-Chem_BC, (c) WRF-Chem_DA, and (d) WRF-Chem_DA_BC.

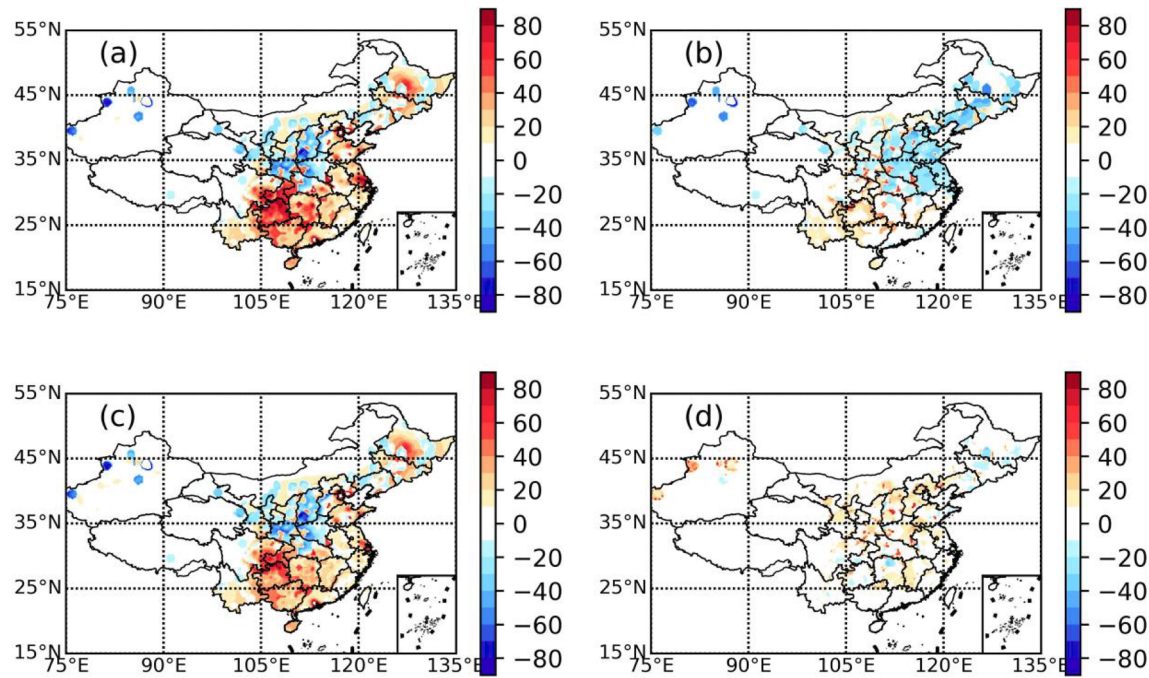


Fig. 4. Spatial distributions of the PM_{2.5} prediction MB ($\mu\text{g}/\text{m}^3$) during winter produced by the four experiments: (a) WRF-Chem, (b) WRF-Chem_BC, (c) WRF-Chem_DA, and (d) WRF-Chem_DA_BC.

3.2. Comparison of the forecast consistency with observations achieved by different optimization methods

The correlation coefficient (R), calculated as in equation (7), can be

used as a criterion to judge the consistency between the model forecast and the observation. Fig. 5 presents the average correlation coefficients between the PM_{2.5} concentration predictions and observations in the four different experiments. The correlation coefficients between the

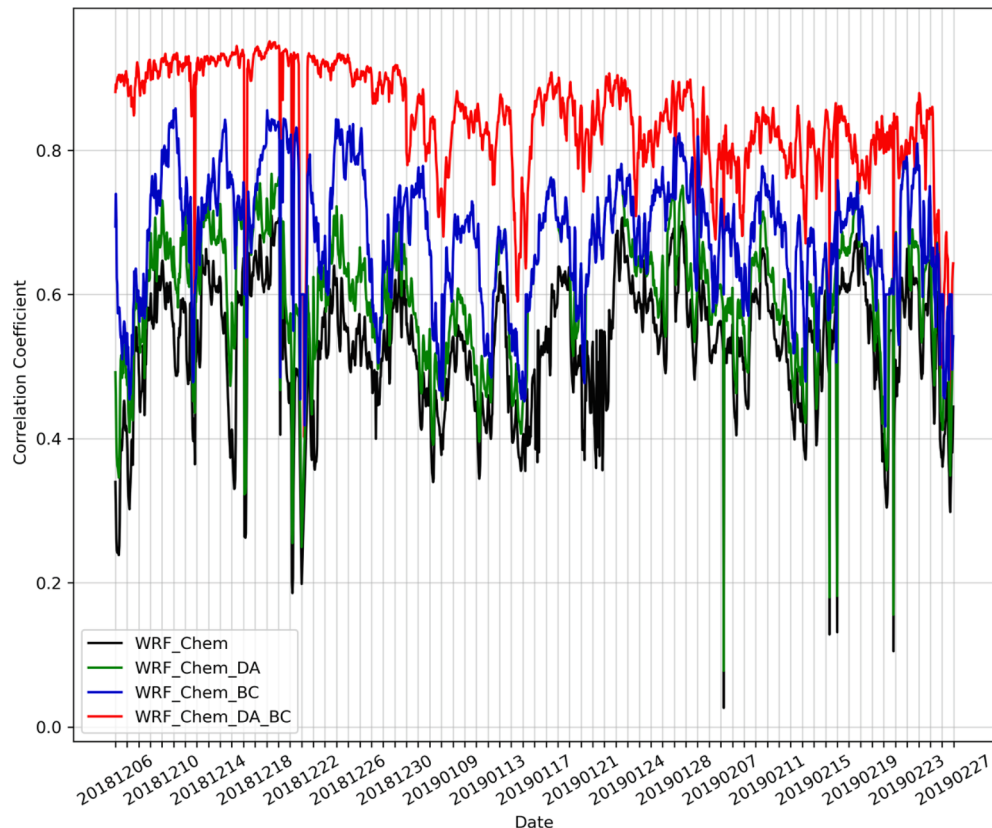


Fig. 5. Temporal variation of the R between observations and the predictions produced by the four experiments: (a) WRF-Chem, (b) WRF-Chem_DA, (c) WRF-Chem_BC, and (d) WRF-Chem_DA_BC.

predictions produced directly by WRF_Chem and observations in the control experiment were in the range of 0.2 to 0.7, which is similar to previous studies (Hong et al., 2022). Both DA and BC were able to improve the consistency of the predictions with the observations, but the optimization effects of the BC method were more effective, with correlation coefficients of 0.4 to 0.8. As can be seen, the predictions produced by WRF-Chem_DA_BC showed the strongest consistency with observations, with R values of 0.7 to 0.85 for most time periods. Therefore, combining DA and BC improved the consistency of the predictions and the observations, and the optimization effect was the best among all the experiments.

The average PM_{2.5} concentrations predicted by the four experiments and observed in the study period are given in Fig. 6. From the scatter fitting analysis results, WRF-Chem_DA_BC performed best in its consistency with observations following optimization. The results predicted directly by WRF-Chem in the control experiment were dispersed, with some isolated overestimation and underestimation scatter points fitted along the slope of 0.56, which demonstrates poor ability in simulating the high-pollution zones. By applying DA, the predictions of WRF-Chem_DA were partially improved, with an increased fitting slope of 0.69, showing less overestimation and underestimation through the adjustment of the initial field. The optimization of WRF-Chem_BC was

much more evident than that of WRF-Chem_DA compared with the control experiment since the overestimation of the model was adjusted and the overall scatter distributions were more concentrated. However, there still existed an overall underestimation trend, with a slope of 0.73 after BC, which may not be sufficient for the simulation of strong pollution processes. It can be seen from Fig. 6a and 6d that the results of WRF-Chem_DA_BC were greatly improved by combining the two optimization methods, with the fitted slope of 1.04 being close to the straight line of $k = 1$. In this experiment, the PM_{2.5} predictions were well adjusted and almost all of the high pollution could be captured, showing the best agreement with the observations. Overall, through adjustment of the model input field and correction of the model output, the predictions were effectively improved. It should be noted that the slope values in the control experiment and WRF-Chem_DA are close to those of previous results (Feng et al., 2018; Ma et al., 2024).

3.3. Influences of the different experimental configurations

To compare the performances of the four experiments, the RMSEs and normalized RMSEs of the PM_{2.5} predictions as functions of forecast range averaged over the whole domain were analyzed.

Fig. 7 shows the regional-average RMSE and normalized RMSE

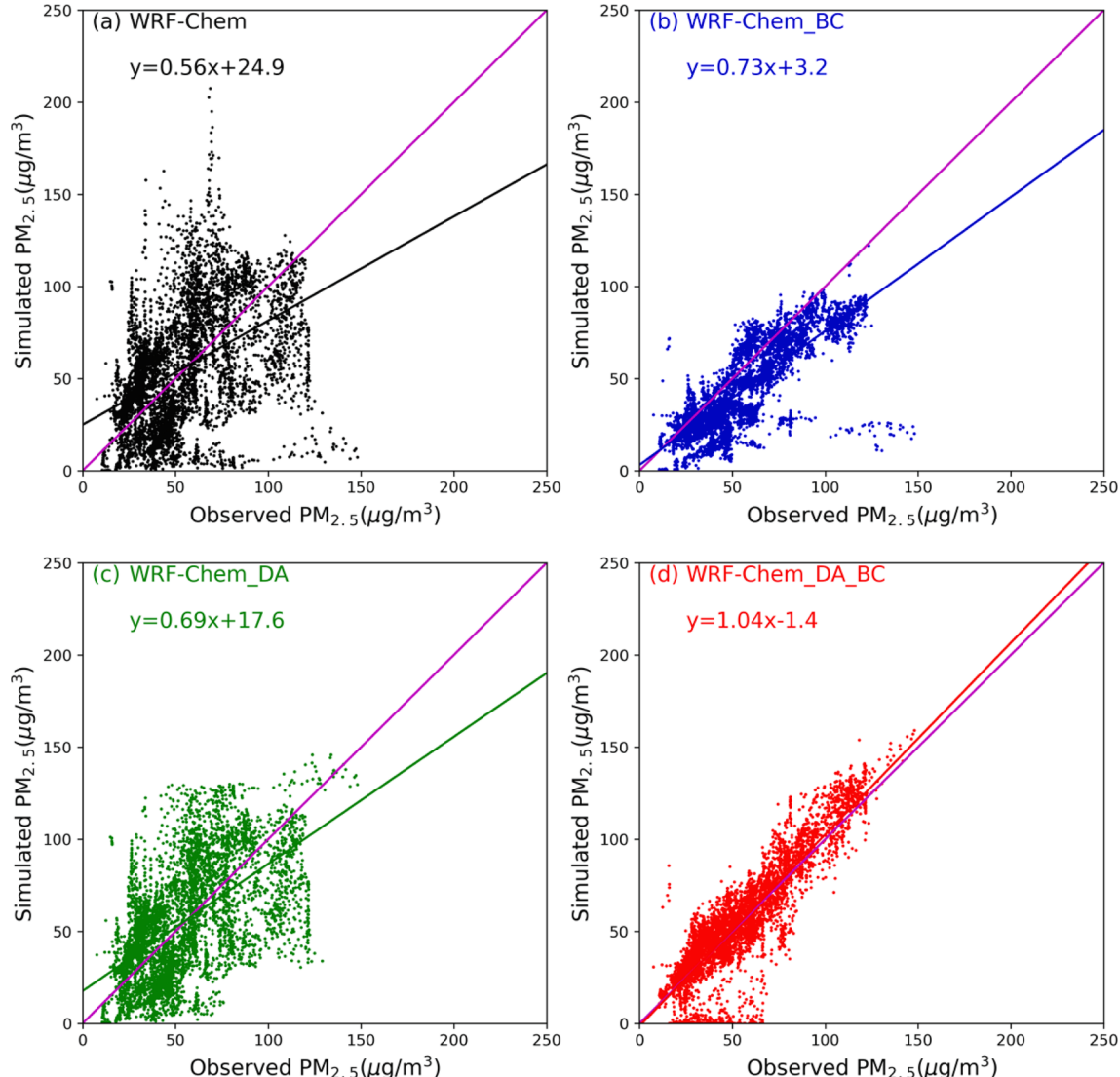


Fig. 6. Scatter plots of simulated versus observed PM_{2.5} mass concentrations ($\mu\text{g}/\text{m}^3$) during winter in the four experiments: (a) WRF-Chem, (b)WRF-Chem_DA, (c) WRF-Chem_BC, and (d)WRF-Chem_DA_BC.

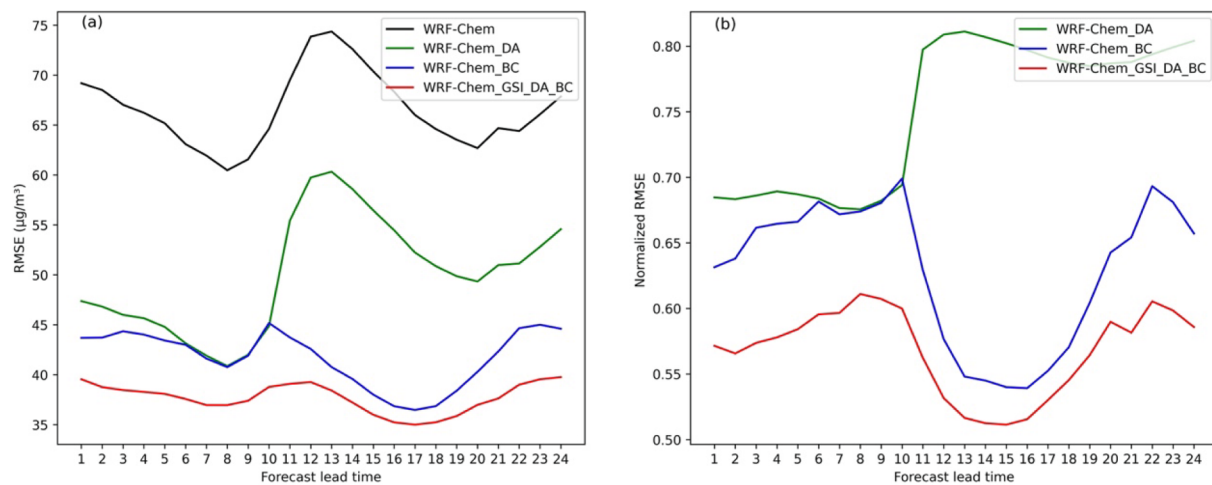


Fig. 7. Hourly averaged (a) RMSE and (b) normalized RMSE of PM_{2.5} predictions with forecasting hour averaged over the entire domain. The black line represents the control experiment; blue, green and red lines represent the WRF-Chem_{BC}, WRF-Chem_{DA} and WRF-Chem_{DA}_{BC} experiments, respectively. (For interpretation of the references to colour in this figure legend, the reader is referred to the web version of this article.)

(RMSEs of the different experiments divided by the RMSE of the control experiment) series of PM_{2.5} predictions with 0–24-h forecasts. It is evident that all three experiments were able to improve the PM_{2.5} predictions in terms of their RMSEs compared with the control experiment. The variations of the RMSE values produced by WRF-Chem and WRF-Chem_{DA} were similar to those in the results of previous studies (Hong et al., 2022; Peng et al., 2018a; Peng et al., 2018b; Ma et al., 2024). Both BC and DA reduced the PM_{2.5} prediction RMSEs throughout the entire 24-h forecasting period, with reductions of 17.89–33.61 μg/m³ and 13.27–21.82 μg/m³, respectively. During the first 0–10 h, the optimization effects of DA and BC were similar, but then BC started to perform better during 10–24 h due to the timeliness of the DA in the initial field, which has also been reported in previous research (Jiang et al., 2013; Ma et al., 2024). Since the optimization of BC was not sensitive to time, the improvement effects could then be maintained, with a normalized RMSE of 0.54 to 0.70, during the 0–24-h forecasting period. Comparatively, WRF-Chem_{DA}_{BC} produced more accurate PM_{2.5} predictions than WRF-Chem_{DA} and WRF-Chem_{BC} during the first 24-h period, with an RMSE reduction of 23.52 to 35.95 μg/m³ owing to the adjustment of the initial field for the model input and the correction of the output at the same time to achieve a double optimization. Overall, despite the positive effects on PM_{2.5} predictions, the optimization achieved by the different experiments varied; specifically, WRF-Chem_{DA}_{BC} was best, followed by WRF-Chem_{BC}, and then finally WRF-Chem_{DA}. The error values of predictions produced by WRF-Chem and WRF-Chem_{DA} were close to some previous DA results in China (Peng et al., 2018a; Peng et al., 2018b; Ma et al., 2024).

The above analysis was made from the perspective of the whole domain in China, and the conclusions reached are that WRF-Chem_{DA}_{BC} adjusted the initial field of the model input on the one hand, while on the other hand it corrected the systematic errors of the model output, thereby evidently improving the PM_{2.5} predictions by simultaneously combining DA and BC. Since the performances of the numerical model varied among different regions, we selected representative urban agglomerations for further analysis that have received attention in previous research (Chen et al., 2022). The RMSE of PM_{2.5} predictions was calculated in each urban agglomeration averaged over the study period, and all the experiments showed improvements compared with the control experiment over these regions. Fig. 8 reveals that the predictions of WRF-Chem_{DA}_{BC} showed better effects than those of WRF-Chem_{DA} and WRF-Chem_{BC} over different urban agglomerations, with a similar trend as in Fig. 7. Notably, the RMSE variations of the PM_{2.5} predictions by WRF-Chem_{DA} and the control experiment were similar during the 0–24-h forecast period, while the daily trend

disappeared by adding the BC in WRF-Chem_{BC} and WRF-Chem_{DA}_{BC}.

From Fig. 3 and Fig. 4, we can see that the prediction RMSEs of the control experiment were relatively larger in BTH due to its underestimation. The improvement of PM_{2.5} predictions in BTH in terms of RMSE reductions by BC were more obvious than those by DA, with regional-average normalized RMSEs of 0.78–0.87 and 0.41–0.72, respectively, which was consistent with the RMSE and MB distributions. From the perspective of the regional-average RMSE, WRF-Chem_{DA}_{BC} produced a reduction in values of 24.74–78.25 μg/m³ due to the combination of DA and BC effects, which shows its advantages over the other experiments in the BTH region. Both DA and BC were able to make adjustments to the overestimation of the PM_{2.5} predictions in the control experiment in YRD and CC. However, despite their similar effects in the first 10 h, the optimization of BC was much better than DA in the later forecasting period since the effects of DA may decrease with the increase in the forecasting period. In SCB, the optimization of DA was not as good as that in CC and YRD due to the larger uncertainty caused by the complex terrain here (Wei et al., 2022), which caused the relatively similar effects of the WRF-Chem_{BC} and WRF-Chem_{DA}_{BC} experiments here. Overall, the effects of DA over YRD and CC were more obvious than over BTH and SCB. BC led to good performances over the whole 0–24-h forecasting period, while DA effects may diminish with the increase in forecasting hours. By combining DA and BC in the WRF-Chem_{DA}_{BC} experiment, the consistency between PM_{2.5} predictions and observations was improved greatly, showing the best forecast effects. The normalized RMSEs produced by WRF-Chem_{DA}_{BC} over BTH, YRD, CC, and SCB were 0.38–0.68, 0.43–0.61, 0.60–0.72, and 0.51–0.70, respectively. These prediction statistics in different regions also indicate the effectiveness and applicability of the combination of BC and DA in improving PM_{2.5} forecasts.

3.4. 2.5. PM_{2.5} prediction results of WRF-Chem_{DA}_{BC}

Section 3.3 confirmed the greater improvement in PM_{2.5} prediction realized by combining the DA and BC methods. Thus, the prediction results produced by the WRF-Chem_{DA}_{BC} experiment are analyzed in the following. Fig. 9a–9c show the results from the control experiment, observation, and WRF-Chem_{DA}_{BC} experiment, respectively. In winter 2019, PM_{2.5} was mainly concentrated over the central-eastern and west-southern regions of China, especially in BTH, Shandong, YRD, CC, and SCB, with the highest values reaching 120 μg/m³, consistent with the distributions reported in other studies (Feng, 2018; Hong et al., 2022). Compared with the *in situ* observations, the overall distributions produced by the control and WRF-Chem_{DA}_{BC} experiments were similar

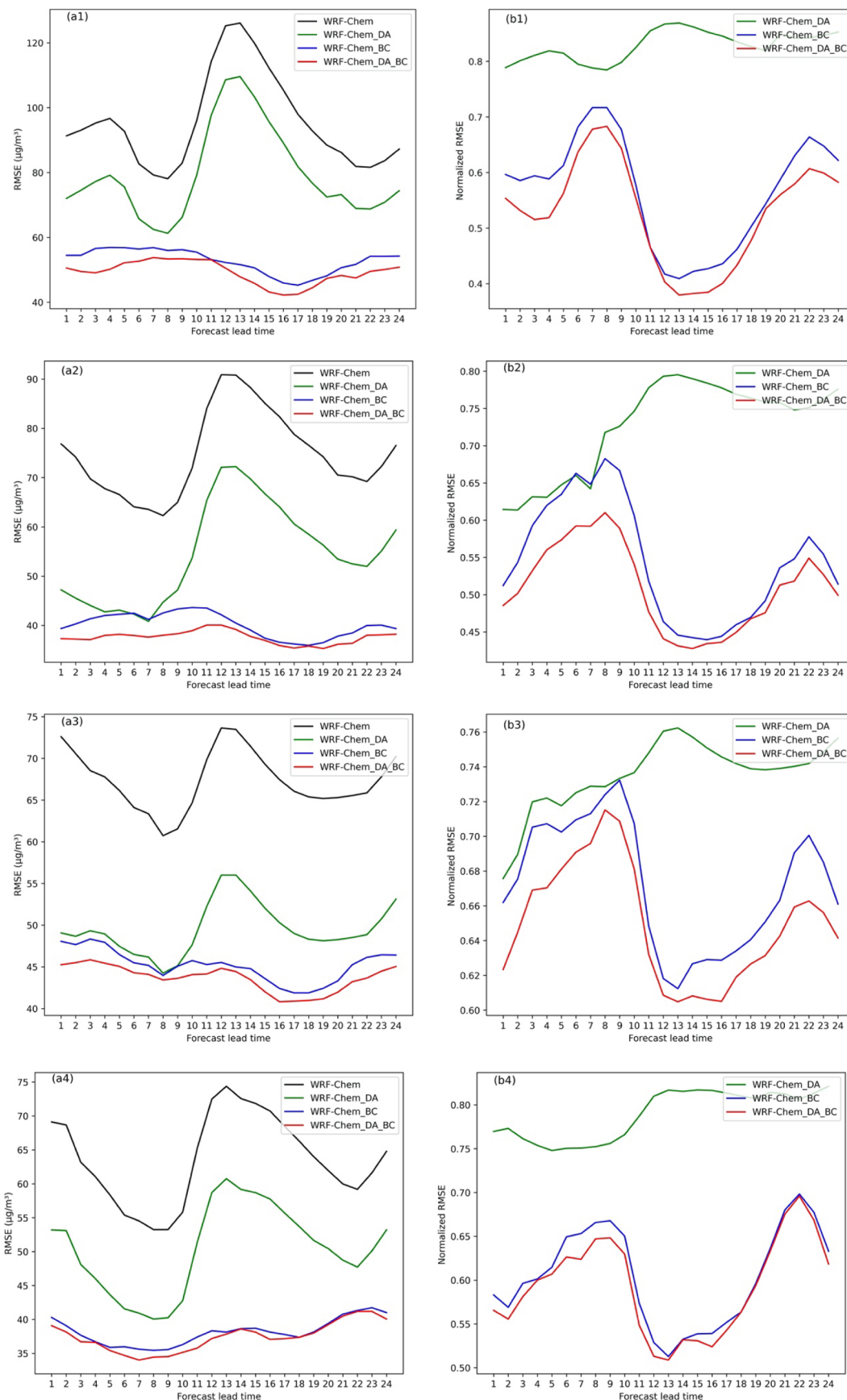


Fig. 8. Hourly averaged RMSE and normalized RMSE of $\text{PM}_{2.5}$ predictions with forecasting hour averaged over (a1, b1) BTB, (a2, b2) YRD, (a3, b3) CC, and (a4, b4) SCB. The black line represents the control experiment; blue, green and red lines represent the WRF-Chem_BC, WRF-Chem_DA and WRF-Chem_DA_BC experiments, respectively. (For interpretation of the references to colour in this figure legend, the reader is referred to the web version of this article.)

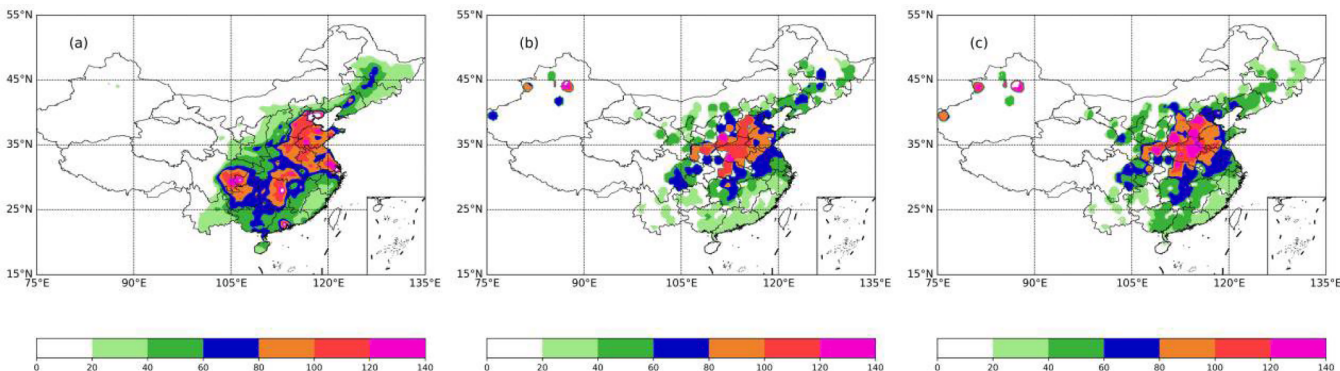


Fig. 9. Spatial distributions of average hourly PM_{2.5} concentrations ($\mu\text{g}/\text{m}^3$) predicted in the (a) control experiment, (b) observations, and (c) WRF-Chem_DA_BC experiment.

over central and eastern China; however, the predictions of WRF-Chem_DA_BC showed better consistency with observations. In the control experiment, PM_{2.5} predictions were largely overestimated over YRD, CC, and around SCB, and underestimated in Shanxi Province, while the WRF-Chem_DA_BC experiment adjusted the concentrations in these regions. By combining the adjustment of the model input and corrections to the model output, the PM_{2.5} prediction distribution and values were much closer to the observations, showing large advantages over these important regions examined in this study (Hong et al., 2022 ; Jiang et al., 2013; Ma et al., 2024). Despite the overall improvement associated with the combined application of DA and BC, there was still little or no improvement over some cities in Northeast China due to the lack of observations, which will need further research.

Urban agglomerations can be severely polluted due to their elevated levels of human activity and other factors, and thus attention to pollution forecasting in these regions is necessary for the management of urban pollution and the development of appropriate strategies. Fig. 10 shows the average atmospheric PM_{2.5} concentration distributions of the

four large urban agglomerations in winter over China investigated in this study. The results show that the concentrations averaged over BTH, YRD, CC, and SCB were 54.53, 55.93, 60.34, and 41.93 $\mu\text{g}/\text{m}^3$, respectively. In total, the concentration of PM_{2.5} in SCB was relatively low. According to the distributions of PM_{2.5}, areas of high PM_{2.5} concentrations in each region were generally in large cities and surrounding areas, close to related emissions linked with human activities.

Time series of the regional-averaged PM_{2.5} predictions over the entire domain and the four urban agglomerations are shown in Figure S1 and Figure S2, respectively. From the figures, we can see that some undulation existed during the pollution processes due to the high incidence of winter haze. The results indicate that WRF-Chem_DA_BC reduced the RMSE, improved the time series consistency, and better captured particular pollution episodes, which is in agreement with the statistical results presented in section 3.3. Despite the overall good performances of WRF-Chem_DA_BC in the four regions, it still underestimated the PM_{2.5} concentrations during a pollution process in February 2019, which may have been caused by the fixed emissions

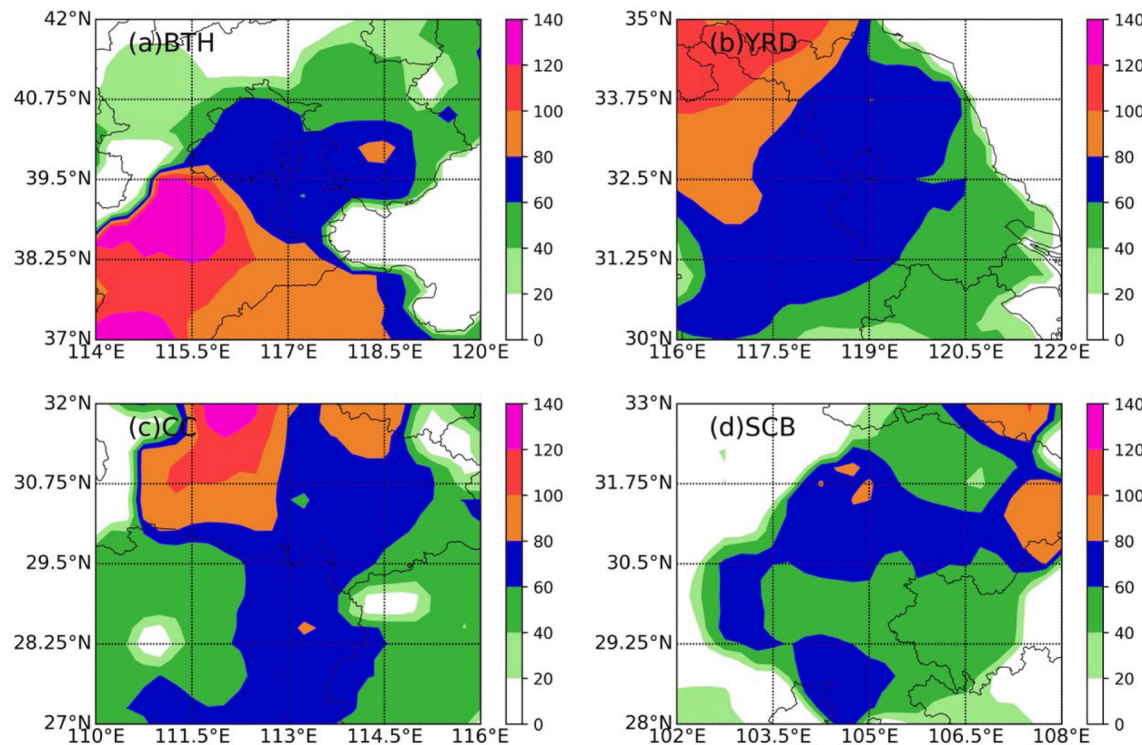


Fig. 10. Distributions of PM_{2.5} concentrations ($\mu\text{g}/\text{m}^3$) predicted in WRF-Chem_DA_BC in four large urban agglomerations in China: (a) BTH; (b) YRD; (c) CC; and (d) SCB.

inventory we used here. Besides, the predictions produced by WRF-Chem_DA_BC revealed better consistency with observations in BTH and YRD. As such, although the predictions were improved in the WRF-Chem_DA_BC experiment, some overestimation errors still existed, with the regional average concentration being 58.84 and 56.86 $\mu\text{g}/\text{m}^3$ for the prediction and observations, respectively. In the current DA experiment, we only considered the adjustment of the initial state of the aerosol fields, without giving concern to the adjustment of emissions, which might have limited the improvement in results.

4. Discussion and summary

4.1. Discussion

Despite the superior performance produced by combining DA and BC, certain aspects still need further discussion. In this study, we only considered the effect of DA through adjustment of the initial aerosol field, which may have had limitations on the optimization effects. The adjustment of emissions has been proved to be critical in terms of the improvement of aerosol predictions in previous studies (Henze et al., 2009; Ku and Park, 2011). As such, greater optimization might be achievable by the additional assimilation of air quality data through applying an inverse method to retrieve an optimized emission inventory based on the model configuration as in the WRF-Chem_DA_BC experiment, which will be analyzed in future work.

In addition, we mainly focused on the effects of the new scheme combining DA on the initial conditions and BC and only considered the DA at 00:00 UTC. To make our findings more robust through further comparisons, we intend to also apply the DA at 06:00, 12:00 and 18:00 in the future research.

Lastly, it should be acknowledged that we mainly compared and analyzed the results of the different experiments in a 0–24-h forecasting period. Since BC is not sensitive to the length of the forecast, long-term predictions can be analyzed in future work. Also, since many methods have been used in the bias correction of numerical models, work will be carried out with other models in the future to make further comparisons with the results reported here.

4.2. Summary

Although many methods have been applied in the adjustment of the initial field and output field to improve $\text{PM}_{2.5}$ concentration predictions, few have considered the combination of DA adjustment and post-processing correction. In this study, the optimization effects of DA in the adjustment of the initial field, and of BC in post-processing, were compared and a new scheme that combined DA and BC simultaneously was developed, showing great advantages in the improvement of $\text{PM}_{2.5}$ concentration predictions. Four parallel experiments were conducted during winter 2019, including a control experiment directly forecasted by WRF-Chem, an experiment that assimilated *in situ* observations based on GSI, an experiment with BC based on MDS-UNet, and an experiment that combined DA and BC.

Both DA and BC improved $\text{PM}_{2.5}$ predictions, but their performances showed differences among regions, indicating the varied effectiveness of these two optimization methods. Through the optimization achieved by DA, the prediction RMSE in WRF-Chem_DA was reduced by 20 to 40 $\mu\text{g}/\text{m}^3$ over CC and YRD compared with the control experiment. The performances of BC were much better than those of DA, showing larger RMSE reductions, and the RMSE values over most areas were less than 80 $\mu\text{g}/\text{m}^3$ in the WRF-Chem_BC experiment.

By combining DA and BC simultaneously, further improvements could be made by integrating the advantages of the two methods. DA improved the prediction accuracy by adjusting the initial field to optimize the model input, while BC made improvements by correcting the biases of the model output, which together realized model optimization from different perspectives. Accordingly, WRF-Chem_DA_BC was able to

utilize the advantages of both DA and BC, thereby benefiting $\text{PM}_{2.5}$ predictions. Overall, WRF-Chem_DA_BC showed the smallest prediction errors, with RMSE values less than 60 $\mu\text{g}/\text{m}^3$ and MB values less than 20 $\mu\text{g}/\text{m}^3$. Besides, it also showed the strongest consistency with observations, with R values of 0.7 to 0.85 for most time periods and a fitted slope of 1.04 close to the straight line of $k = 1$.

From the perspective of regionally averaged and normalized RMSEs during the 0–24-h forecasting period, all experiments had positive effects on $\text{PM}_{2.5}$ predictions, but the optimization of WRF-Chem_DA_BC was best, with the RMSE reduced by 23.52 to 35.95 $\mu\text{g}/\text{m}^3$, followed by WRF-Chem_BC and then WRF-Chem_DA. The normalized RMSEs produced by WRF-Chem_DA_BC over BTH, YRD, CC, and SCB were 0.38–0.68, 0.43–0.61, 0.60–0.72, and 0.51–0.70, respectively.

The averaged $\text{PM}_{2.5}$ distributions in winter revealed that $\text{PM}_{2.5}$ predictions were notably overestimated over YRD and CC and around SCB in the control experiment, whereas the WRF-Chem_DA_BC experiment adjusted the concentrations in these regions. The concentrations averaged over BTH, YRD, CC, and SCB were 54.53, 55.93, 60.34, and 41.93 $\mu\text{g}/\text{m}^3$, respectively, which were close to the values in other studies. WRF-Chem_BC_DA better captured particular pollution episodes, but it still underestimated the $\text{PM}_{2.5}$ concentrations during a pollution process in February 2019, possibly because of the fixed emissions inventory we used here. In the current DA experiment, we only considered adjustment of the initial state of the aerosol fields, without giving concern to the adjustment of emissions, which might have limited the improvement in results.

CRediT authorship contribution statement

Xingxing Ma: Writing – original draft, Validation, Software, Methodology, Conceptualization. **Hongnian Liu:** Writing – review & editing, Resources, Funding acquisition. **Zhen Peng:** Investigation, Funding acquisition.

Declaration of competing interest

The authors declare that they have no known competing financial interests or personal relationships that could have appeared to influence the work reported in this paper.

Acknowledgments

This study was supported by the National Natural Science Foundation of China (U2342221). The numerical calculations conducted for this study were performed at the High-Performance Computing Center at Nanjing University. We acknowledge the use of both the WRF-Chem model, which is available at <https://github.com/wrf-chem>, and the MEIC emissions data, which are provided by the MEIC group at www.meicmodel.org. We would also like to thank both the European Centre for Medium-Range Weather Forecasts (<http://apps.ecmwf.int/datasets/>) for providing the ERA5 reanalysis data, and the China Environmental Monitoring Centre (<http://106.37.208.233:20035>) for providing the surface $\text{PM}_{2.5}$ data.

Data availability

Data will be made available on request.

References

- Bocquén, M., Elbern, H., Eskes, H., et al., 2015. Data assimilation in atmospheric chemistry models: current status and future prospects for coupled chemistry-meteorology models. *Atmos. Chem. Phys.* 15 (10), 5325–5358.
- Chen, F., Dudhia, J., 2001. Coupling an advanced land surface hydrology model with the Penn State/NCAR MM5 modeling system. Part I: model implementation and sensitivity. *Mwr* 129 (4), 569–585.

- Chen, D., Liu, X., Lang, J., et al., 2017. Estimating the contribution of regional transport to PM_{2.5} air pollution in a rural area on the North China Plain. *Sci. Total Environ.* 583, 280–291.
- Chen, B., Song, Z.H., Huang, J.P., et al., 2022. Estimation of atmospheric PM₁₀ concentration in China using an interpretable deep learning model and top-of-the-atmosphere reflectance data from China's new generation geostationary meteorological satellite, FY-4A. *J. Geophys. Res. Atmos.* 127 (9).
- Chen, S.Q., Xu, J.J., Zhang, Y., Shen, W.Q., Guan, Z.Y., Dong, C.M., 2023. Impact of GPS radio occultation assimilation on the 18–21 July 2021 heavy rainfall event in Henan. *Atmos. Res.* 286, 106661. <https://doi.org/10.1016/j.atmosres.2023.106661>.
- Chin, M., Ginoux, P., Kinne, S., Torres, O., Holben, B.N., Duncan, B.N., et al., 2002. Tropospheric aerosol optical thickness from the GOCART model and comparisons with satellite and Sun photometer measurements. *J. Atmos. Sci.* 59 (3), 461–483.
- Dudhia, J., 1989. Numerical study of convection observed during the winter monsoon experiment using a mesoscale two-dimensional model. *J. Atmos. Sci.* 46 (20), 3077–3107.
- Evensen, G., 2009. Data assimilation: the ensemble Kalman filter[M]. Springer Science & Business Media, City.
- Feng, S.Z., 2018. Study for Impact of Data Assimilation on PM_{2.5} Forecast [D].
- FU Y., LI R., HU J., et al. Investigating the impacts of satellite fire observation accuracy on the top-down nitrogen oxides emission estimation in northeastern Asia. *Environment International*, 2022, 169: 107498.
- Feng, S.Z., Jiang, F., Jiang, Z.Q., et al., 2018. Impact of 3DVAR assimilation of surface PM_{2.5} observations on PM_{2.5} forecasts over China during winter time [J]. *Atmos. Environ.* 187, 34–49.
- Gao, W.K., Tang, G.Q., Ji, D.S., et al., 2016. Implementation Effects and Countermeasures of China's Air Pollution Prevention and Control Action Plan [J]. *Res. Environ. Sci.* CNKI:SUN:HJKX.0.2016-11-001.
- Glahn, H.R., Lowry, D.A., 1972. The use of model output statistics (MOS) in objective weather forecasting [J]. *J. Appl. Meteor.* 11, 1203–1211.
- Grell, G.A., Peckham, S.E., Schmitz, R., McKeen, S.A., Frost, G., Skamarock, W.C., et al., 2005. Fully coupled “online”_chemistry within the WRF model. *Atmos. Environ.* 39 (37), 6957–6975.
- Guenther, A., Karl, T., Harley, P., Wiedinmyer, C., Palmer, P.I., Geron, C., 2006. Estimates of global terrestrial isoprene emissions using MEGAN (Model of Emissions of gases and Aerosols from Nature). *Atmos. Chem. Phys.* 6 (11), 3181–3210.
- Guo, H., Cheng, T., Gu, X., Wang, Y., Chen, H., Bao, F., Meng, C., 2017. Assessment of PM_{2.5} concentrations and exposure throughout China using ground observations. *Sci. Total Environ.* 601, 1024–1030.
- Henze, D.K., Seinfeld, J.H., Shindell, D.T., 2009. Inverse modeling and mapping US air quality influences of inorganic PM_{2.5} precursor emissions using the adjoint of GEOS-Chem. *Atmos. Chem. Phys.* 9 (16), 5877–5903.
- Hong, J., Mao, F., Gong, W., et al., 2022. Assimilating Fengyun-4A Observations to Improve WRF-Chem. PM_(2.5) Predictions in China. *Atmospheric research*, p. 265 (Jan.).
- Hong, S.Y., Noh, Y., Dudhia, J., 2006. A new vertical diffusion package with an explicit treatment of entrainment processes. *Mwr* 134 (9), 2318.
- Jiang Z Q, Liu Z Q, Wang T J, et al. 2013b. Probing into the impact of 3DVAR assimilation of surface PM₁₀ observations over China using process analysis. *Journal of Geophysical Research-Atmospheres*, 118(12): 6738-6749.
- Jiang, F., Liu, Q., Huang, X., et al., 2012. Regional modeling of secondary organic aerosol over China using WRF/Chem. *J. Aerosol Sci.* 43 (1), 57–73.
- Kampa, M., Castanas, E., 2008. Human health effects of air pollution. *Environ. Pollut.* 151 (2), 362–367.
- Klein, W.H., Lewins, B.M., Enger, I., 1959. Objective prediction of five-day mean temperatures during winter [J]. *J. Meteor.* 16, 672–682.
- Ku, B.Y., Park, R.J., 2011. Inverse modelling analysis of soil dust sources over East Asia. *Atmos. Environ.* 45, 5903–5912. <https://doi.org/10.1016/j.atmosenv.2011.06.078>.
- Li, T.W., Yang, Q.Q., Yuan, W., 2023. Joint estimation of PM_{2.5} and O₃ over China using a knowledge-informed neural network. *Geosci. Front.* 14 (2), 101499 <https://doi.org/10.1016/j.gsfs.2022.101499>.
- Li, M., Liu, H., Geng, G., Hong, C., Liu, F., Song, Y., Tong, D., Zheng, B., Cui, H., Man, H., Zhang, Q., He, K., 2017. Anthropogenic emission inventories in China: a review. *Natl. Sci. Rev.* 4, 834–866. <https://doi.org/10.1093/nsr/nwx150>.
- Liu, Jingqi and Jia Xing, “Identifying Contributors to PM_{2.5} Simulation Biases of Chemical Transport Model Using Fully Connected Neural Networks.” *Journal of Advances in Modeling Earth Systems* 15 (2022): n. pag.
- Li, J., Wei, P., Dai, X.Z., et al., 2021. Optimization of Numerical Methods Simulation in Xi'an Based on Machine Learning [J]. *Res. Environ. Sci.* 34 (4), 872–881.
- Lu, J., Xing, J., 2022b. Identifying contributors to PM_{2.5} simulation biases of chemical transport model using fully connected neural networks. *J. Adv. Model. Earth Syst.* 15, e2021MS002898.
- Lu, H., Xie, M., Wu, Z., et al., 2020. Adjusting PM_{2.5} prediction of the numerical air quality forecast, model based on machine learning methods in Chengyu region [J]. *Acta Scientiae Circumstantiae* 40 (12), 4419–4431.
- Ma, X., Liu, H., & Peng, Z. (2024). Assimilating a blended dataset of satellite-based estimations and in situ observations to improve WRF-Chem PM_{2.5} prediction. *In Atmospheric Environment*. doi: 10.1016/J.ATMOSENV.2023.120284.
- Lv, M.Y., Cheng, X.H., Zhang, H.D., et al., 2018. Improving the correction method of air pollutant forecasts from the CUACE model based on the adapting partial least square regression technique [J]. *Acta Sci. Circum.* 38 (7), 2735–2745.
- Ma, C.Q., 2020. Study of Atmospheric Chemistry Data Assimilation based on Ensemble Kalman Filter [D]. Nanjing University.
- Ma, J.H., Cao, Y., Yu, Z.Q., et al., 2020. The application of deep learning method in Shanghai PM_{2.5} prediction [J]. *China Environ. Sci.* 40 (2), 530–538.
- Ma, C., Wang, T., Zang, Z., et al., 2018. Comparisons of Three-Dimensional Variational Data Assimilation and Model Output Statistics in Improving Atmospheric Chemistry Forecasts. *Adv. Atmos. Sci.* 35 (7), 813–825.
- Marzban, C., 2003. Neural networks for post-processing model output: ARPS [J]. *Mon. Wea. Rev.* 131 (6), 1103–1111.
- Malware, E.J., Taubman, S.J., Brown, P.D., Iacono, M.J., Clough, S.A., 1997. Radiative transfer for inhomogeneous atmospheres: RRTM, a validated correlated-k model for the longwave. *J. Geophys. Res.* 102 (14), 16663–16682.
- Morrison, H., Thompson, G., Tatarkii, V., 2009. Impact of cloud microphysics on the development of trailing stratiform precipitation in a simulated squall line: comparison of one- and two-moment schemes. *Mwr* 137 (3), 991–1007.
- Pagowski, M., Liu, Z., Grell, G.A., Hu, M., Lin, H.C., Schwartz, C.S., 2014. Implementation of aerosol assimilation in Gridpoint Statistical Interpolation (v. 3.2) and WRF-Chem (v. 3.4.1). *Geosci. Model Dev* 7 (4), 1621–1627.
- Peng, Z., Liu, Z., Chen, D., Ban, J., 2017. Improving PM_{2.5} forecast over China by the joint adjustment of initial conditions and source emissions with an ensemble Kalman filter. *Atmospheric Chemistry Physics* 17, 4837–4855.
- Peng, Z., Lei, L., Liu, Z., et al., 2018a. The impact of multi-species surface chemical observation assimilation on air quality forecasts in China. *Atmos. Chem. Phys.* 18 (23), 17387–17404. <https://doi.org/10.5194/acp-18-17387-2018>.
- Peng, Z., Lei, L., Liu, Z., et al., 2018b. The impact of multi-species surface chemical observation assimilation on air quality forecasts in China. *Atmos. Chem. Phys.* 18 (23).
- Pope III, C.A., Burnett, R.T., Turner, M.C., Cohen, A., Krewski, D., Jerrett, M., et al., 2011. Lung cancer and cardiovascular disease mortality associated with ambient air pollution and cigarette smoke: shape of the exposure-response relationships. *Environ. Health Perspect.* 119 (11), 1616–1621.
- Qin, C.F., Sun, J.R., Zhang, W.J., et al., 2020. Formation Mechanism of a Large-Scale Heavy Pollution Process in North China in Winter Based on Numerical Simulation and Statistical Fitting [J]. *Clim. Environ. Res.* 25 (2), 185–198.
- Rabier, F., McNally, A., Andersson, E., Coutier, P., Unden, P., Eyre, J., Hollingsworth, A., Bouttier, F., 1998. The ECMWF implementation of three-dimensional variational assimilation (3D-Var). II: structure functions. *Q. J. Roy. Meteorol. Soc.* 124, 1809–1829.
- Raftery, A.E., Gneiting, T., Balabdaoui, F., et al., 2005. Using bayesian model averaging to calibrate forecast ensembles. *Mon. Weather Rev.* 133 (5), 1155–1174.
- Ran, Q., Moore, J., Dong, T., Lee, S.-Y., & Dong, W. (2023). Statistical bias correction for CESM-simulated PM_{2.5}. *Environmental Research Communications*, 5(10), Article 101001. doi: 10.1088/2515-7620/acf917.
- Ronneberger, O., Fischer, P., Brox, T., 2015. U-Net: Convolutional Networks for Biomedical Image Segmentation[G]//International Conference on Medical Image Computing and Computer-Assisted Intervention. Springer International Publishing. https://doi.org/10.1007/978-3-319-24574-4_28.
- Schwartz, C.S., Liu, Z.Q., Lin, H.C., et al., 2012. Simultaneous three-dimensional variational assimilation of surface fine particulate matter and MODIS aerosol optical depth. *J. Geophys. Res. Atmos.* 117 (D13), D13202. doi: 10.1029/2011JD017383. -D13202-22.
- Shen, F., & Min, J. (2015). Assimilating AMSU-A radiance data with the WRF Hybrid En3DVAR system for track predictions of Typhoon Megi (2010). *Advances in Atmospheric Sciences*, 32(9), 1231–1243.
- Shen, F., Xu, D., Xue, M., & Min, J. (2018). A comparison between EDA-EnVar and ETKF-EnVar data assimilation techniques using radar observations at convective scales through a case study of Hurricane Ike (2008). *Meteorology and Atmospheric Physics*, 130(6), 649–666.
- Shen, F., Xu, D., Min, J., Chu, Z., & Li, X. (2020). Assimilation of radar radial velocity data with the WRF hybrid 4DEnVar system for the prediction of hurricane Ike (2008). *Atmospheric Research*, 234, 104771.
- Song, J.K., Chen, Y.D., Chen, D., 2021. A study of meteorology-aerosol joint data assimilation on autumn PM_{2.5} concentration simulation. *Acta Meteorol. Sin.* 79 (3), 477–491.
- Stockwell, W.R., Middleton, P., Chang, J.S., Tang, X., 1990. The second generation regional acid deposition model chemical mechanism for regional air quality modeling. *J. Geophys. Res.* 95 (D10), 16343–16367.
- Mengfan Teng, Siwei Li, Jie Yang, Shuo Wang, Chunying Fan, Yu Ding, Jiaxin Dong, Hao Lin, Shansi Wang. Long-term PM_{2.5} concentration prediction based on improved empirical mode decomposition and deep neural network combined with noise reduction auto-encoder: A case study in Beijing. *Journal of Cleaner Production*, Volume 428, 2023, 139449, ISSN 0959-6526.
- Tie, X., Geng, F., Peng, L., et al., 2009. Measurement and Modeling of O₃ Variability in Shanghai, China: Application of the WRF-Chem Model. *Atmos. Environ.* 43, 4289–4302.
- Van Loon, M., Vautard, R., Schaap, M., et al., 2007. Evaluation of long-term ozone simulations from seven regional air quality models and their ensemble[J]. *Atmos. Environ.* 41 (10), 2083–2097.
- Wang, X.M., Chen, W.H., Chen, D.H., et al., 2016. Long-term trends of fine particulate matter and chemical composition in the Pearl River Delta Economic Zone (PRDEZ), China. *Front. Environ. Sci. Eng.* 10 (1), 53–62.
- Wang, Z., Maeda, T., Hayashi, M., et al., 2001. A nested air quality prediction modeling system for urban and regional scales: Application for high-ozone episode in Taiwan [J]. *Water, Air, Soil Pollut.* 130 (1–4), 391–396.
- Wang, P., Zhang, H., Qin, Z., Zhang, G., 2017. A novel hybrid-Garch model based on ARIMA and SVM for PM_{2.5} concentrations forecasting. *Atmos. Pollut. Res.* 8 (5), 850–860.
- Wei, Y., Zhao, X.J., Zhang, Z.Y., et al., 2022. PM_{2.5} and PM₁₀ data assimilation experiments in China based on the WRFDA-chem three-dimensional variational

- (3DVAR) system. Clim. Environ. Res. 27 (5), 653–668. <https://doi.org/10.3878/j.issn.1006-9585.2021.21109shu> in Chinese.
- You, J.H., 2014. Ensemble Forecasting of Haze in Shanghai [D]. East China Normal University.
- Zeng, Q., Wu, L., 2022. Optimal reduction of anthropogenic emissions for air pollution control and the retrieval of emission source from observed pollutants III: Emission source inversion using a double correction iterative method. Sci. China Earth Sci. 65, 553–555.
- Zhang, Y.B., Chen, M.X., Han, L., et al., 2022. Multi-element deep learning fusion correction method for numerical weather prediction [J]. Acta Meteorol. Sin. 80 (1), 153–167.
- Zheng, B., Tong, D., Li, M., Liu, F., Hong, C., Geng, G., Li, H., Li, X., Peng, L., Qi, J., Yan, L., Zhang, Y., Zhao, H., Zheng, Y., He, K., Zhang, Q., 2018. Trends in China's anthropogenic emissions since 2010 as the consequence of clean air actions. Atmos. Chem. Phys. 18, 14095–14111. <https://doi.org/10.5194/acp-18-14095-2018>.
- Zhou G, Yang F, Geng F, et al. 2015. Measuring and modeling aerosol: relationship with haze events. in Shanghai, China. Aerosol Air Qual. Res., 14:783–792,2014.
- Zhu, Y., Luo, Y., 2015. Precipitation calibration based on the frequency-matching method. Weather Forecast. 30 (5), 1109–1124.
- Zhu, J., Tang, X., Wang, Z.F., et al., 2018. A review of air quality data assimilation methods and their application [J]. Chin. J. Atmos. Sci. 42 (3), 607–620.